

# Evaluation of the pore morphology formation of the Freeze Foaming process by *in situ* computed tomography

Matthias Ahlhelm<sup>1</sup>, David Werner<sup>1</sup>, Johanna Maier<sup>2</sup>, Johannes Abel<sup>1</sup>, Thomas Behnisch<sup>2</sup>, Tassilo Moritz<sup>1</sup>, Alexander Michaelis<sup>1</sup>, Maik Gude<sup>2</sup>

<sup>1</sup>Fraunhofer Institute for Ceramic Technologies and Systems, IKTS, Winterbergstraße 28, 01277 Dresden, Germany

<sup>2</sup>Technische Universität Dresden, Institute of Lightweight Engineering and Polymer Technology, Holbeinstr. 3, 01307 Dresden, Germany

## Abstract:

The so-called Freeze Foaming method aims at manufacturing ceramic cellular scaffolds for diverse applications. One application is dedicated to potential bone replacement material featuring open, micro and interconnected porosity. However, the main challenges of this foaming method is to achieve a homogeneous pore morphology. In a current project, the authors throw light on the bubble/pore and strut formation of this process by *in situ* computed tomography. This allows for evaluating varying process parameter's effects on the growth of the ceramic foam during the foaming process. As first result and basis for CT analysis, a stable and reproducible model suspension was developed which resulted in reproducible foam structures. In dependence of selected process parameters like pressure reduction rate or air content in the ceramic suspension resulting Freeze Foams became adjustable with regard to their pore morphology. Pore size and distribution data as well as the porosity were characterized and evaluated accordingly.

**Keywords:** Freeze Foaming; Bioceramics; Foaming process; *in-situ* CT; None destructive testing

## 1. Introduction

### 1.1 The Freeze Foaming process

There is a variety of foaming techniques of ceramic suspensions. The two largest industrially relevant techniques are based on poly urethane (PU) foam replication (Replica/Schwartzwalder approach [1]) and pore forming substances like e.g. starch, wax, polymeric beads, carbon black or sawdust [2,3]. PU scaffold and pore formers later need to be burned out in order to achieve the desired porous body. By a third relevant technique, the direct foaming, suspensions are foamed either by turbulent mixing with surfactants [4] or by *in situ* gas and vapour developing reactions [5,6].

In contrast to these foaming techniques that are based on the burnout of organic volatile pore formers and polymer scaffolds, the so-called Freeze Foaming is the direct foaming of almost any desired material (diverse ceramics, metals, etc.) prepared as aqueous suspension. Without foaming agents or deliberately injected gas into a suspension, the Freeze Foaming process is triggered by ambient pressure reduction of an aqueous suspension in a freeze dryer. Through the applied vacuum, the suspension medium inflates by rising processing air and water vapour. Further pressure reduction drives the aqueous system along the vapour-liquid equilibrium line towards the triple point (p,T-diagram of water, Figure 1, II). When that point is crossed, the generated proto foam freezes instantaneously and subsequently dries via sublimation (Figure 1, III-IV) [7,8]. Thus, the Freeze Foam's pore formers are rising bubbles of processing air and water vapour as well as sublimated frozen water.

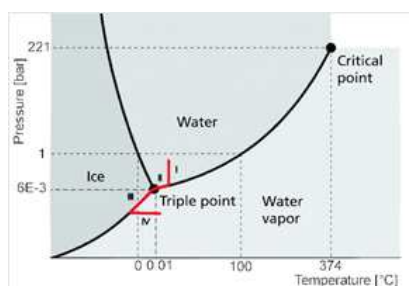


Figure 1: Exemplary p,T-phase diagram of water including Freeze Foaming process [8].

Those structures are then debinded and sintered. Resulting Freeze Foams typically exhibit filled struts and a high proportion of open porosity, micro porosity and interconnectivity. An example of a highly porous sintered hydroxyapatite foam is shown in Figure 2.

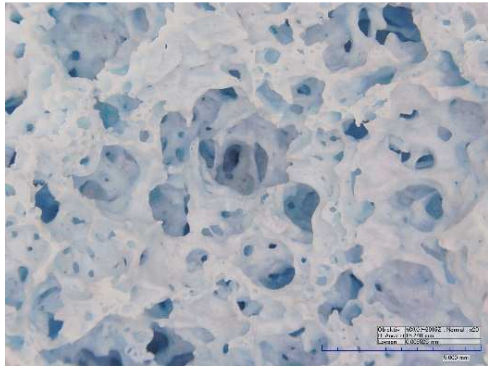


Figure 2. Optical microscopic image of an open porous sintered hydroxyapatite Freeze Foam.

Especially these are properties, which demonstrably predestine such cellular structured Freeze Foams for a possible use as biocompatible components when made of Hydroxyapatite (HAp) or  $ZrO_2$ ; even as composite mixture [9-11]. In addition, Freeze Foaming offers near-net shaping capabilities and was also applied to develop porous refractory bricks made of mullite [12,13]. In recent contributions, the Freeze Foaming's advantages were used to fill the inside of 3-dimensional, complex-shaped hollow shell geometries. Those shell structures can be manufactured either by conventional or by Additive Manufacturing processes. In that way, porous and cellular features provided by the Freeze Foaming have been connected to dense and complex features provided by LCM (Lithography-based Ceramic Manufacturing). Demonstrators in form of a femoral bone model were successfully co-sintered to one composite part. This hybrid shaping technology therefore offers a wide range of application potential for personalized and surface customizable implant structures to be applied in the field of biomedical technology and engineering [14,15] (Figure 3).

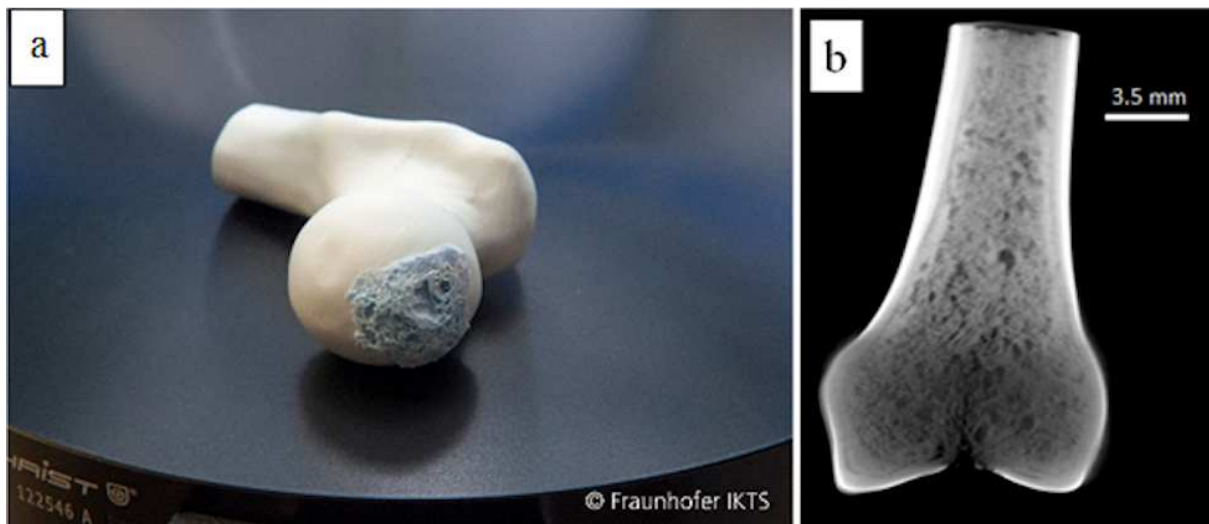


Figure 3. Hybrid shaping approach to bone-mimicking scaffolds: a) femoral bone model of HAp, b) CT reconstruction images of a bone model made of  $ZrO_2$ .

The above mentioned examples so far were made only on a laboratory scale. An upscaling of the Freeze Foaming process requires larger batches of ceramic suspensions. Suspension and Freeze Foaming need to be reproducible and robust. Industry often requires foamed scaffolds to have either a closed or open as well as a homogeneous pore morphology in order to guarantee and provide the targeted properties. For instance, refractories require homogeneously distributed small pores (mainly closed porosity) in the range of 100 nm to 1mm for proper isolation capability [16]. With regard to bioceramic scaffolds for bone replacement material, a porosity greater than 70-80 %, interconnectivity [17] and sufficiently large pores (at least 100-500  $\mu\text{m}$ ) for cell attachment [18, 19] as well as micro porosity is required [20]. Like depicted above, Freeze Foaming indeed allows producing open porous,

interconnected and microporous scaffolds. However, on the example of Figure 2 and Figure 3b a completely heterogeneous pore morphology becomes obvious. That makes estimations and assessment concerning the reproducibility of biocompatibility and even mechanical strength very difficult.

Therefore, intense research is needed with regard to establishing a material preparation and process approach that firstly, allows a controlled tuning of the pore morphology and secondly, provides real time data acquisition of the foaming process, the strut and bubble/pore formation itself.

## 1.2 *In situ* computed tomography

*In situ* analyses allow insights into processes that have an influence on materials, for instance during preparation, occurring reactions or under load. One solution is being provided by computed tomography (CT) and *in situ* computed tomography which has become a sophisticated tool for improved damage and degradation analyses in the field of material sciences [21-25]. An additional and important advantage is the allocation of 3-dimensional (3D) volumetric pore morphology information. Software tools like MAVI [26] or VGStudio Max [27] give access to volume-based data like porosity, pore size and distribution or pore shape. This contribution reports about the use of *in situ* CT to acquire and clarify occurring Freeze Foaming phenomena and to derive the key principles of foaming process. The results shall allow the production of 3D scaffolds with targeted pore size and distribution.

Within the frame of a DFG-funded project (“Erarbeitung der Gesetzmäßigkeiten der Schaumstrukturbildung im Gefrierschäumprozess biokompatibler Keramikschaume”) CT analyses are provided by the project partner *Technical University Dresden, ILK (Institute for Lightweight Engineering and Polymer Technology), TUD-ILK*. The analyses of the evolving foam structure by X-ray measurements will be conducted by two methods: the first is real-time foaming monitoring by X-ray radiography (2D), the second method, allowing the evaluation of foam structuring phenomena, is computer-aided reconstruction of areal image information by means of  $\mu$ CT (3D) [28,29]. In order to gather 3D foam volume information by CT scan (usually 3-10 minutes for one measurement) the foaming process itself needs to be stopped at certain points. Accordingly, adapted equipment is necessary to regulate and even stop/fixate the foaming e.g. by pressure control.

This contribution gives first insights into the current project and its preliminary results. The focus first was laid on manufacturing a stable and reproducible model suspension, which has to tolerate the transport to the project partner and behave (foam) as identical as possible. Only this allows an equally-as-possible foaming process under controlled and specific conditions within the provided CT experimental setup. We then varied process parameters (pressure reduction rate, air content) to observe their effects on the pore morphology and derive principles of the Freeze Foaming process.

## 2. Materials and methods

Hydroxyapatite (Co. Sigma-Aldrich, BET = 70.01 m<sup>2</sup>/g, d<sub>50</sub> = 2.64 μm) was chosen as ceramic biomaterial. The prepared ceramic suspensions comprise the powder, polyvinyl alcohol as binder, Dolapix CE 64 (Co. Zschimmer & Schwarz) as dispersing agent and the rheological modifier (Tafigel PUR40, Co. Münzing GmbH). Based on previous work a suspension composition suitable for stable foaming process was chosen and optimized according to: rheological behaviour suited for mold filling, foaming and green body stability as well as porosities of foamed specimen (green bodies) of < 70-80 %. Within a diploma thesis, first experiments were carried out accordingly.

The following processing route was conducted: Deionized water was mixed manually with dispersing agent (2 vol.-%). Subsequently, the ceramic powder (28 vol.-%) was added, followed by the polyvinyl alcoholic binder (13% aqueous solution) and rheological modifier (8 vol.-%). This mixture was then stirred manually (to pre-mix binder and powder components) prior to be transferred into a centrifugal vacuum mixer (Thinky ARV310). The prepared mixture was exposed to a high stirring rate (2000 rpm, mixing time 2x1 minute, with ZrO<sub>2</sub> mixing spheres) in order to disperse the particles and reduce agglomeration. The obtained suspension was cooled down until reaching room temperature. After those preliminary steps, always the same amount of suspension (2 g) was filled into a mold (cylindrical, 14 mm diameter x 20 mm height) and transferred to the freeze dryer (Lyo Alpha 2-4, LSCplus, Co. Martin Christ GmbH) to be freeze-foamed.

For microstructure analysis the freeze-foamed bodies were characterized by SEM (Ultra 55, Co. Carl Zeiss). The geometrically derived porosities were calculated according to  $P = 1 - \frac{\rho_{th}}{\rho_{bulk}}$ . For X-Ray radiography and  $\mu$ CT a Phoenix v|tome|x L 450 (Fa. GE Sensing & Inspection Technologies) and a FCTS 160 – IS (Fa. FineTec FineFocus Technologies GmbH) were used.

## 2.1 Experimental setup

In a first experimental setup, it should be tested whether or not the pressure rate has an effect on the foaming process and its resulting structures. Vacuum was initiated with a pressure reduction rate of 10 mbar/s down to about 20 mbar. From here we proceeded down to the triple point, firstly with the same relatively slow rate of 10 mbar/s and secondly at a very fast rate given by the automated pressure control of the Lyo Alpha 2-4 (Figure 4).

20 mbar as turning point was chosen because prior monitoring of the Freeze Foaming process with product sensors and subsequent process evaluation using the freeze dryer's internal monitoring software LyoLogplus showed two sections of the foaming: one down to 30 mbar being escaping dissolved processing air only and the other from 30 to 6 mbar being water vapour. In order to observe effects of either air-derived foaming or vapor-derived foaming individually we later degassed a set of suspensions. They most likely weren't fully degassed though. The little quantity of suspensions allowed only an experimental setup in which the pressure reduction was exerted whilst mixing the suspension in the centrifugal vacuum mixer (120 mbar for 60 min). Applying more vacuum already would have caused water vapor to escape. The accordingly treated suspension are further referred to as degassed suspensions.

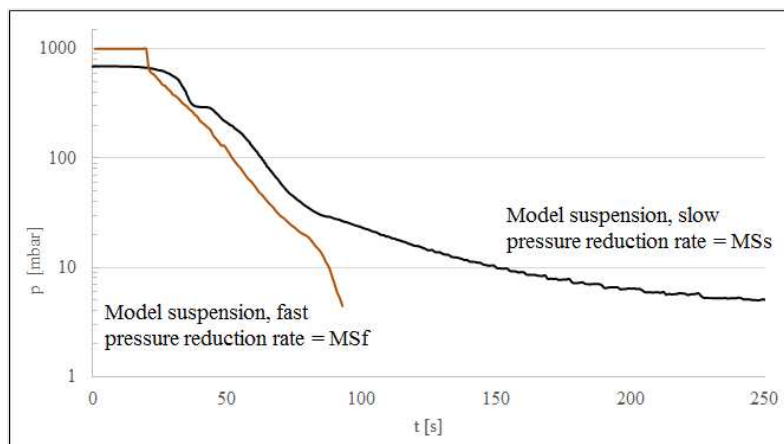


Figure 4. Visible representation of the foaming process's two pressure reduction rates.

## 3. Results and Discussion

As mentioned earlier, we firstly concentrated on the development of a reproducible model suspension. At first stage of the project we didn't so much focus on achieving one defined pore size but rather on observing and clarifying the phenomena of the Freeze Foaming. However, we already aimed at reaching a pore size range from around 100-700  $\mu$ m as well as a homogenous distribution of pores. In addition, achieved porosities should be greater than 70-80% and mainly feature interconnectivity in order to achieve pore morphologic properties generally meeting the requirements for bone replacement material (see section 1.1 page 2). According to compositions based on previous projects, suspensions were prepared with varying amount of water known for having one of the main effects on the Freeze Foaming process. After developing a model suspension resulting foams need to be evaluated regarding their porosity and microstructure in dependence on the exerted process parameters, which there are: slow pressure reduction rate on a model suspension (MSs), fast pressure reduction rate on a model suspension (MSf) and the same for the degassed model suspensions (MSs\_d, MSf\_d). The following chapters primarily concentrate on the green-state foams since this condition directly represents the structural evolution at the end of the Freeze Foaming process.

### 3.1 Development of a model suspension

A stable foaming process takes place firstly, when the volume of the suspension significantly increases, secondly, when there is no pulsation at maximum foaming height and thirdly, when the foam does not collapse. It was found that if the amount of water in the suspension is lower than 35 wt.-%, the obtained high viscous mixture inhibits growth of air and water vapour bubbles. Foam does not grow uniformly and only very little in height with only a few pores and more dense sections (Fig. 5, No. 2). Instead, the optimal concentration of water lies within 35-38 wt.-% (around 62 Vol.-%). Obtained viscous suspensions allow a stable foaming to an overall porous foam structure (Fig. 5, No. 3). In the case of increasing the water content to more than 39 wt.-%, the suspension has a too low viscosity resulting in an unstable foaming process, completely collapsing foams and a very randomized and heterogeneous pore structure (Fig. 5, No. 4).

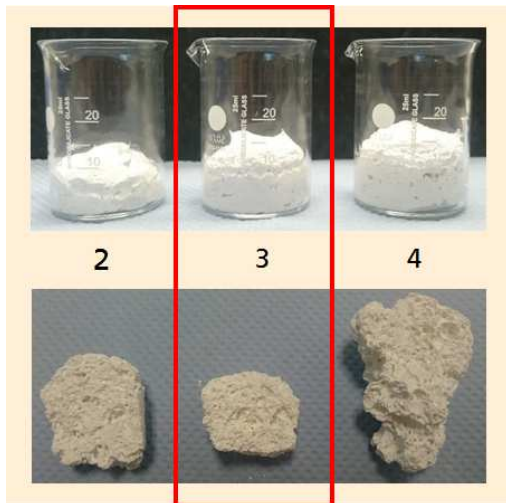


Figure 5. Visualisation and choice of a stable Freeze Foaming process on the example of a hydroxyapatite foam.

Therefore, suspensions with 62 vol.-% liquid phase were chosen with respect to a stable foaming result in combination with processing and flow behaviour, which is important for later mold filling. As mentioned earlier, reproducibility of foam structures is the most important aspect for the ongoing project. Therefore, the same suspension was manufactured at least five times and its rheological behaviour determined. As it turned out, the viscosity behaved very similar, indeed almost identical for the normal model suspension as well as for the degassed suspension (Figure 6 left and right).

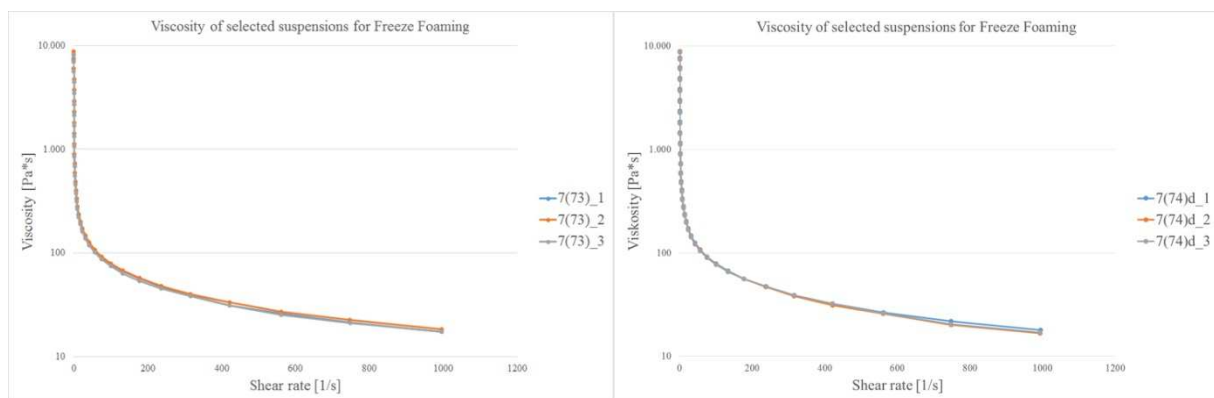


Figure 6. Viscosity comparison of the Freeze Foam model suspension, left: suspensions with dissolved air, right: degassed suspensions.

More importantly, the foamed suspensions, now Freeze Foams in green state (Figure 7), showed a very similar porosity with a mean value of 86.2 % (Table 1) proving, that it is possible to achieve a stable and reproducible model suspension yielding Freeze Foams with quite similar porosities. Height and diameter was measured at three sections of each Freeze Foam and the according mean values calculated to receive the porosity data. This model suspension (in normal and degassed condition), was later used to be foamed at the *TUD-ILK* facilities, too.



Figure 7. Manufactured model Freeze Foams (green state).

Table 1 Example of reproducibility experiments of selected green-state Freeze Foam's porosities (geometrically determined from cylindrical foams).

Sample name	d1 [mm]	d2 [mm]	d3 [mm]	Mean d [mm]	h1 [mm]	h2 [mm]	h3 [mm]	Mean h [mm]	Porosity [%]
11_1	14.89	14.71	14.85	14.82	17.45	17.36	16.50	17.10	85,49
11_2	14.80	14.69	14.82	14.77	15.96	15.10	15.50	15.52	84,47
11_3	14.58	14.51	14.60	14.56	21.94	20.85	22.50	21.76	86,95
11_4	14.80	14.89	14.75	14.81	15.05	15.45	14.58	15.03	86,24
12_1	14.76	14.80	14.60	14.72	16.41	16.10	16.84	16.45	86,58
12_2	14.80	14.79	14.75	14.78	16.56	17.20	15.95	16.57	86,46
12_3	14.21	14.35	14.41	14.32	19.69	19.21	19.84	19.58	85,24
12_4	14.63	14.52	14.74	14.63	18.10	18.56	17.95	18.20	86,29
13_1	14.66	14.38	14.12	14.39	17.78	17.51	18.12	17.80	84,44
13_2	14.71	14.69	14.95	14.78	19.90	20.12	20.55	20.19	87,02
13_3	14.70	14.58	14.85	14.71	21.23	21.14	22.10	21.49	86,70
13_4	14.72	14.35	14.75	14.61	18.54	18.88	19.21	18.88	85,55
14_1	14.53	14.87	14.69	14.70	18.87	19.29	19.97	19.38	86,71
14_2	14.38	14.73	14.69	14.60	17.56	18.62	18.01	18.06	85,52
14_3	14.78	14.70	14.68	14.72	21.53	21.03	21.49	21.35	86,41
14_4	14.66	14.21	14.86	14.58	23.67	23.21	23.97	23.62	85,31
47_1	14.76	15.11	15.07	14.98	23.76	23.71	22.71	23.39	87,98
47_2	14.58	14.6	14.69	14.62	20.65	20.39	20.85	20.63	87,76
47_3	13.94	14.53	14.8	14.42	22.84	22.72	22.63	22.73	86,34
47_4	14.76	14.63	14.6	14.66	20.07	20.52	20.16	20.25	86,52

								Mean porosity	86,2
								Standard deviation	0,9

### 3.2 The microstructure of obtained Freeze Foams

All Freeze Foams were analysed with regard to their microstructure and porosity mainly by means of CT and SEM measurements (green state foams were ion-polished in order to keep the fragile green state intact). Figure 8 shows indeed a dependency of the porosity of foamed suspensions at different pressure reduction rate (three foams per pressure rate were evaluated). With a fast pressure reduction rate, the porosity is around 3 % higher than obtained Freeze Foams foamed with the slow pressure reduction rate. However, since the mean deviation for the latter lies within the porosity of the fast pressure reduction rate this result should be regarded critically.

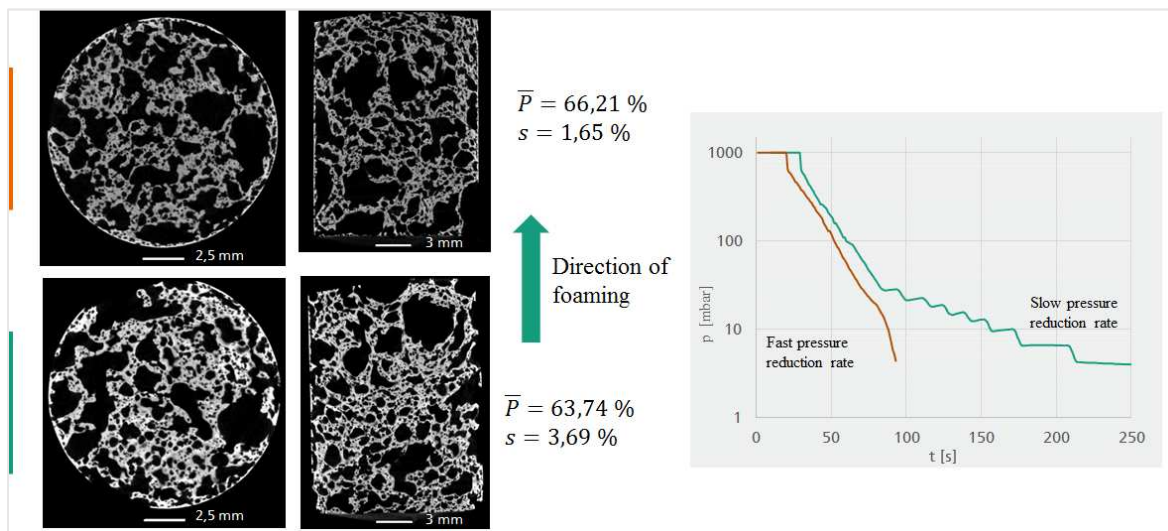


Figure 8. CT cross-section images and pressure rate depending porosity of selected Freeze Foams.

#### 3.2.1 SEM analyses

The green-state Freeze Foams made with normal and degassed model suspensions by fast and by slow pressure reduction rate foaming were now compared to each other with regard to their microstructure. At this early project's stage, only a fraction of available Freeze Foams have been evaluated. Therefore, shown images and according results need to be handled deliberately.

Figure 9 shows the example of a Freeze Foam's microstructure at fast pressure reduction rate (MSf) versus slow pressure reduction rate (MSs). Already differences can be noted: at fast pressure reduction rate (Figure 9, left) the majority of smaller pores (100-600  $\mu\text{m}$ ) are still slightly spherical and plenty in abundance. Some of them seem to be in a condition of *pre-coalescence* and *pre-Ostwald ripening* (air bubbles connecting to each other evening out inner partial pressure and ripening to bigger bubbles, later pores, with less surface tension/inner partial pressure). These spherical pores lie in between pore walls/struts of around 200-400  $\mu\text{m}$  thickness. These struts itself are filled as well as microporous and connect large elongated macro pores of several hundreds of micrometre in size (up to 1-2 mm). In contrast, at slow pressure reduction rate (Figure 9, right) the rising bubbles of dissolved air dwell longer in a pre-frozen state (before 6 mbar) in comparison to fast pressure reduction, therefore starting to clearly destabilize whilst the suspension is foaming. The majority of pores is elongated, also the smaller pores (150-400  $\mu\text{m}$ ) which are conglomerated in joined clusters of several millimetres in size. In addition, these kind of pores is reduced in number. The struts (70-1200  $\mu\text{m}$  thick) are still microporous connecting further larger elongated macropores. Already visible at fast pressure reduction rate now at slow pressure reduction rate, single larger pores (100-600  $\mu\text{m}$ ) are surrounded by microporous material in the struts. In areas with more pores within the struts, the material obviously looks denser (brighter in the SEM images). Here, the many evolving bubbles probably have squeezed

and therefore densified the material between them and thus, causing the observed density inhomogeneity.

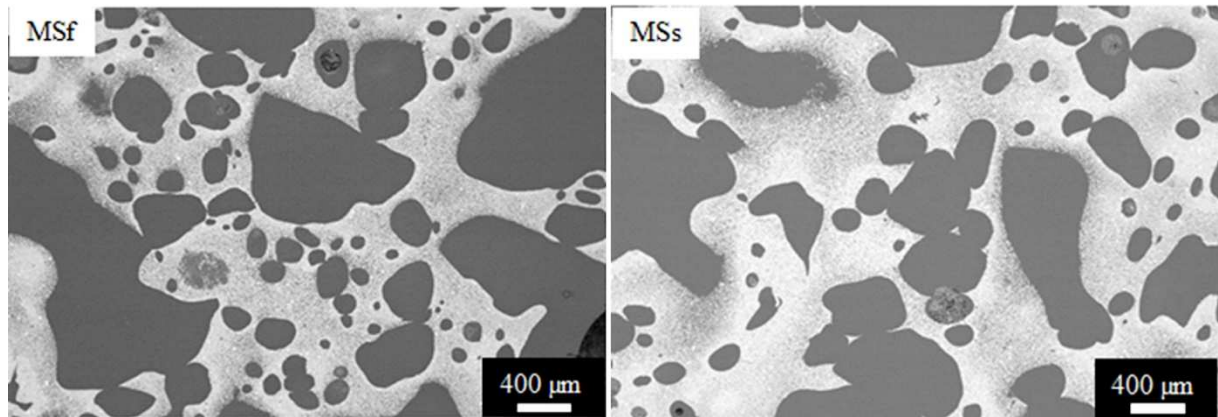


Figure 9. SEM microstructure comparison of normal model suspension's Freeze Foams (green state) foamed at fast (MSf) and slow pressure reduction rate (MSs).

Taking a closer look at the foamed degassed suspensions, Figure 10 clearly shows a significant increase in a microporous structure within the struts, caused by sublimation of frozen water, now looking similar to cryogenic textures. This cryogenic micro porosity evolves into dendritic looking channel-like structures when foaming a degassed suspension at slow pressure rate (MSs\_d, Figure 10, right). The obtained Freeze Foam's microstructure is characterized by ragged struts (200-1000 μm), mainly irregular pores (300 μm-several millimetres) and large pore connecting struts with crossing cracks. Since these cracks are also visible in degassed suspension-derived foams which have not yet been machined an external damaging caused e.g. by the preparation of samples for SEM analyses, is ruled out.

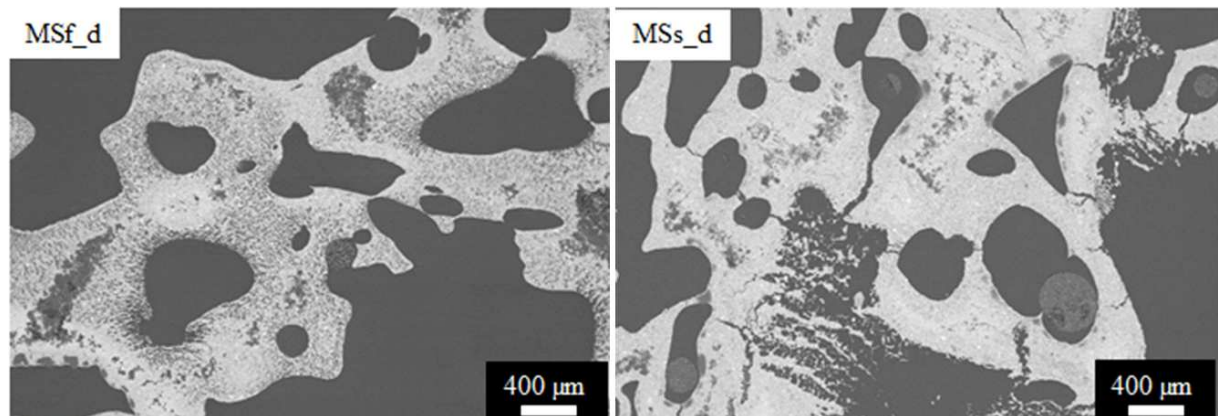


Figure 10. SEM microstructure comparison of degassed suspension's Freeze Foams (green state) foamed at fast (MSf\_d) and slow pressure reduction rate (MSs\_d).

Concerning the degassed suspension, another pore-forming mechanism seems to be of significance or rather comes to the fore. As it was stated at the beginning, the pore forming regions can be distinguished into air and water vapour-based pores. So far, we weren't able to get any quantitative data (e.g. density measurement comparisons of the suspensions were carried out) but the degassed suspension must have another air content (presumably less) than a normal suspension because a different foaming behaviour was observed. There seems to be a pore morphology influencing mechanism at work, which needs further attention. For that, we come up with the following theory (based on those preliminary results): process-induced and dissolved gases in the normal model suspension account to the foaming of mainly spherical pores (up to 400 μm) up to around 100 mbar ambient pressure at fast pressure reduction rate. The time for destabilizing effects such as coalescence and Ostwald ripening to occur is relatively short. These destabilizing effects are becoming more significant though, when foaming at slower pressure reduction rates. The abundance of pores accounts

to a certain (also interconnected) porosity through which the remaining water can evaporate relatively fast at the end of the foaming process (20-6 mbar). In contrast, the foaming of degassed suspensions results in a coarser and much more macroscopic structure, which becomes significantly rugged and cracked at low-pressure reduction rate foaming. At this stage, we suggest water vapour instantaneously being released during sublimation to be the source of defects. In contrast to the normal suspension featuring (more) air bubbles-induced porosity the now released water vapour cannot be transported fast enough through now less pores and hence, induces cracks. However, more samples need to be tested in order to prove that theory and to get a statistical significance.

### 3.2.2 Computed tomographic analyses

A number of green foams were analysed via  $\mu$ -CT at the *TUD-ILK* to further evaluate the microstructure. The resolution was adjusted to 9.7 voxel. The software VGStudio Max v. 3.0 was used to determine the pore size distribution of scanned foams. As operational procedure, first a “Region of Interest” was defined (ROI, Figure 11, top left). Then the surface was determined. The grey value defines material and material’s border indicated as grey regions respectively a white line (Figure 11, top right). Dark regions reflect air/pores. A following defect analysis shows the identified foam cells, marked yellow (Figure 11, bottom left). The last step is the foam structure analysis (Figure 11, bottom right) determining isolated pores (foam cells with no connection to neighbouring cells) and connected pores (contact to at least one neighbouring foam cell by a cell window). The colour indicates the volume size of the foam’s pores (blue to red with increasing volume). The threshold for the segmentation of connected foam pores was adjusted to 50 %. The resulting pore volume  $V$  was transformed to the equivalent ball diameter  $d$  by the equation:  $d = \left(\frac{6V}{\pi}\right)^{\frac{1}{3}}$ . Due to the resolution the smallest pore has a diameter of 24  $\mu\text{m}$ .

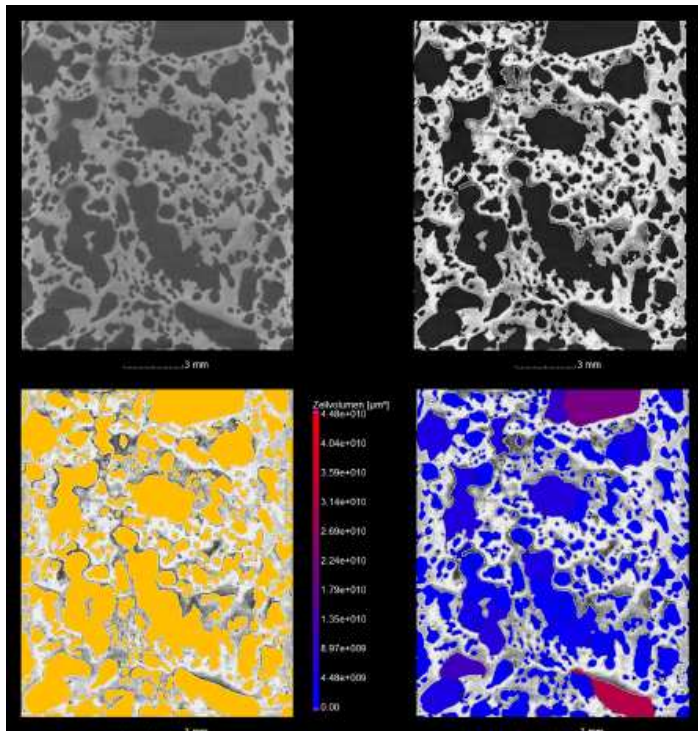


Figure 11. Foam structure analysis procedure (VGStudio Max v. 3.0) on the example of a degassed model suspension foamed at slow pressure reduction rate (MSs\_d), cutting plane parallel to foaming direction.

In the following figure (Figure 12), isolated and connected pores were combined to display the pore size distribution of Freeze Foams originating from normal and degassed (\_g) model suspension as well as foamed at a fast and slow pressure reduction rate (MSs, MSf).

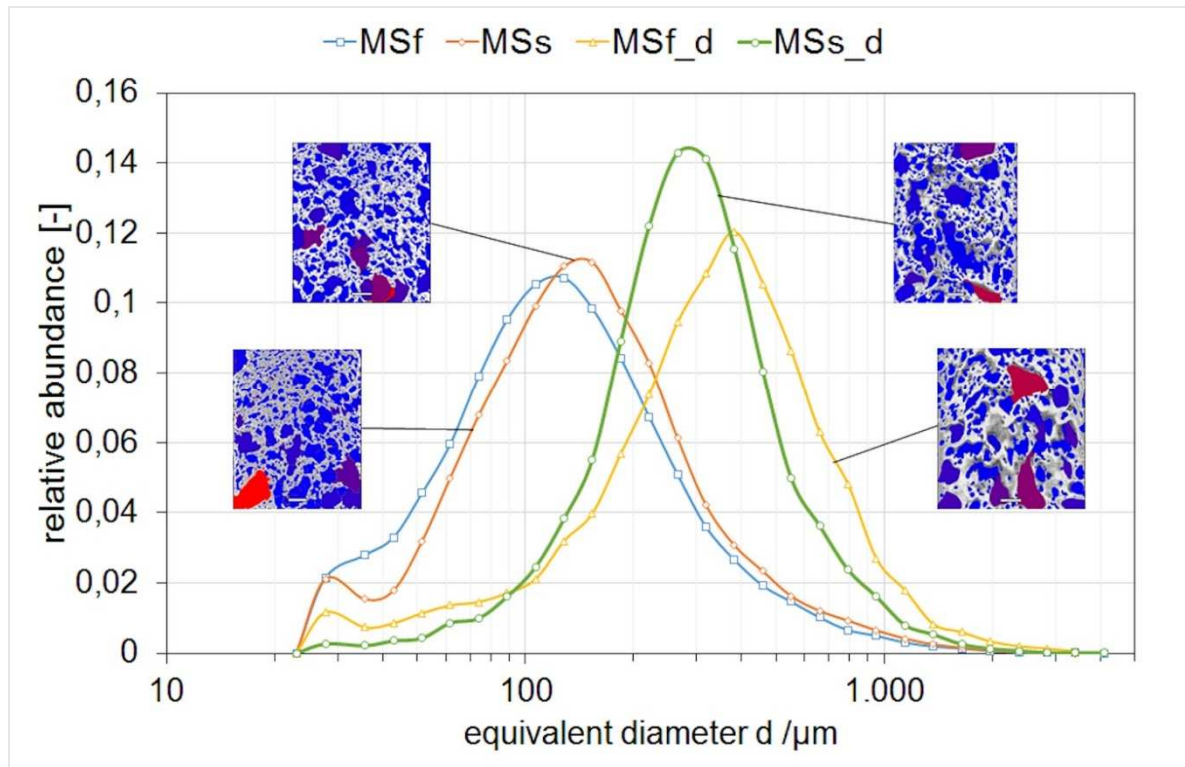


Figure 12. Foam structure analysis-derived comparison of pore size distribution of normal and degassed model suspensions at fast (MSf) and slow pressure reduction rate (MSs).

It is obvious that the green-state scaffolds foamed on basis of the normal model suspension significantly differ from the ones foamed from the degassed model suspension. In accordance to the SEM image analyses and therefore proving the stated consideration, the degassed suspensions result in foams featuring much bigger pores. Moreover, the fast pressure reduction rate results in larger pores (peak around 380  $\mu\text{m}$ ) in comparison to the slow pressure reduction rate (around 270  $\mu\text{m}$ ). In contrast, the normal suspension foamed scaffolds have their maximum abundance of pores at a size of around 150  $\mu\text{m}$  for the slow pressure reduction rate and around 130  $\mu\text{m}$  for the fast pressure reduction rate. Also in accordance with the SEM analysis, both normal suspension-derived foams exhibit a higher number of smaller pores (25-70  $\mu\text{m}$ ) than the degassed suspension-derived foam. Table 2 summarizes the median of the pore sizes (calculated on basis of three foams for each changed suspension/process parameter). The average median of MSf and MSs is very close to each other and lies within the deviation. In accordance to the figure above MSf\_d features larger pores than MSs\_d.

Table 2. Process parameter dependant pore size distribution-derived median of obtained Freeze Foams (green state).

		Median [ $\mu\text{m}$ ]	Average [ $\mu\text{m}$ ]	Standard deviation
MSf	7(47)5	130	128	6
	7(14)2	119		
	7(47)4	134		
MSs	7(55)3	123	131	6
	7(55)6	137		
	7(55)8	133		
MSf_d	7(60)4	235	358	23
	7(60)5	335		
	7(60)6	381		
MSs_d	7(59)2	223	261	27

### 3.3 First in situ CT analyses at TUD-ILK

Figure 13 depicts the experimental setup for the *in situ* Freeze Foaming analyses at TUD-ILK. The foaming takes place in a vacuum chamber very similar to the freeze dryer, only much smaller. Within that chamber the stable foaming of the model suspensions takes place. Pressure sensor, control valve and bypass allow a monitored pressure rate variation to determine possible effects on the pore morphology during the Freeze Foaming. The structural changes during foaming are analysed either by the in-line operating R $\mu$ CT or by X-ray radiography.

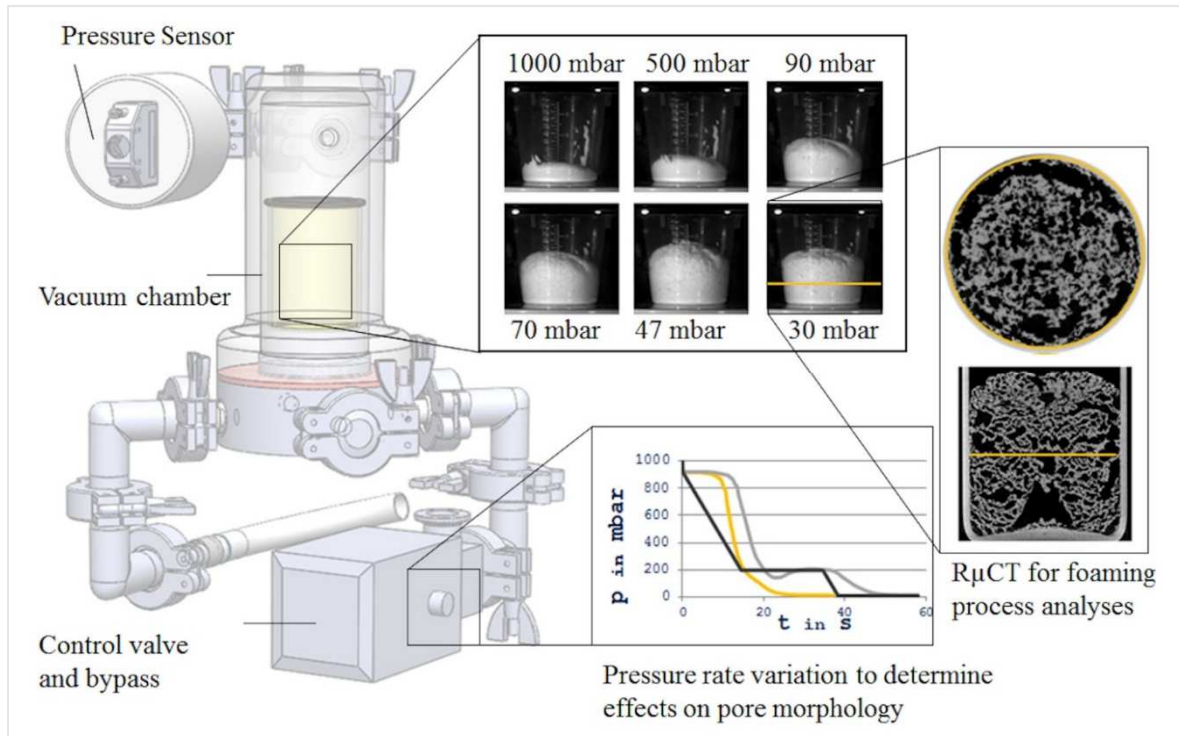


Figure 13. Experimental in situ CT setup for the Freeze Foaming process at TUD-ILK.

The first experiments with varying pressure rates at 10, 30 and 50 mbar/s show the development of similar looking, highly and heterogeneously porous Freeze Foams (Figure 14). Porosity analyses show the increase in porosity from process start (liquid suspension) to process end (frozen stable Freeze Foam) at a rate of 10 mbar/s pressure rate being quadrupled, at 30 mbar/s featuring 4.5 times the starting condition's porosity and at 50 mbar/s 5 times porosity. The most striking features though are the large and irregular shaped pores which dominate the foam structures.

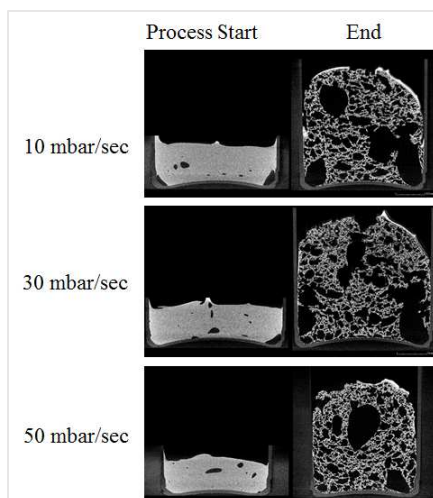


Figure 14. Pressure rate variation and effect on Freeze Foam pore morphology analysed by CT measurement.

Taking a closer look at the CT images it became obvious that “voids” of air already enclosed in the suspensions finally evolved into those dominant, large macroscopic pores (coloured marks in Figure 15). These results hint to factors so far little regarded: the filling procedure of a mold and size- and geometry-related effects on the later foam structures. Compared to the molds used at the IKTS (15 mm in diameter and 20 mm in height) the molds used at *TUD-ILK* were much bigger (approximately 25 mm in diameter, 50 mm in height) and not flat at the bottom but concave. We assume that the size of a mold influences the foaming process. A large aspect ratio mold potentially results in a more horizontal oriented pore structure whereas a small aspect ratio mold results in a vertical elongated pore structure. Comparing Figure 11 (foaming in cylindrical mold of 14 mm in diameter) with Figure 14 and Figure 15 seems to confirm this assumption (with the exception of the large voids). However more samples need to be tested in order to systematically investigate and verify mold geometry-related influences on the Freeze Foaming process.

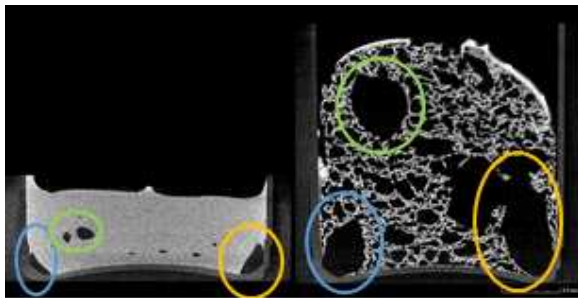


Figure 15. Exemplary evolution of pores during the Freeze Foaming process as result of CT measurement.

#### 4. Summary and Outlook

In the first period of this DFG-funded project, we succeeded in developing a reproducible model suspension suitable for a stable and reproducible Freeze Foaming process. This model suspension was the scrupulous basis for manufacturing reproducible foam structures (foamed at IKTS) and later also in-situ CT analyses at the project partner’s facilities. A regulation of material (air content in the suspension) and process parameters (pressure reduction rate) allowed us to influence and adjust the pore morphology of manufactured Freeze Foams. The results of pore size and porosity evaluation generally meet the requirements for bone replacement material as was targeted at. By use of computed tomographic analyses we were able to reveal material/process parameter-dependent structure development phenomena (pore formation) and derive the first principles of the Freeze Foaming process.

We come up with the following conclusions:

1. The Freeze Foaming process can be divided into two pore forming sections, one ruled by dissolved air in the suspension (taking place until around 20 mbar) and the other ruled by evaporating water taking place from 20 to 6 mbar ambient pressure.
2. Depending on the amount of dissolved gases in the suspension, the resulting Freeze Foams also differ in their microstructure. Less air seems to promote the development of larger cryogenic even dendritic structures whereas a normal amount of air (usual processing) results in more and smaller spherical pores.
3. The faster the pressure reduction rate the larger and more irregular the pores become.
4. As shown by first in-situ CT analyses, the porosity of Freeze Foams increases with increased pressure reduction rate.
5. As shown by first in-situ CT analyses, the geometry of the mold and probably the filling procedure (possibility of enclosed air in the suspension) has an effect on the pore structure of obtained Freeze Foams and needs further consideration.

This contribution is mainly about green-state Freeze Foams, which is useful and necessary in terms of evaluating the foaming method's effects on the resulting pore structure as-foamed. It is the sintered foams though which will play their role in application. They will be analysed next accordingly and in comparison to their green state condition.

In the following period of this project, we aim at further understanding the highly active foaming section identified at a pressure of around 100 mbar to 20 mbar and making visible the effects of the Freeze Foaming's process manipulation by means of radiographic analyses. A pressure reduction rate will be chosen, which seems the most promising in terms of a stable foaming process (resulting in a homogenous as possible pore structure). Already in process are the evaluation of the sintered Freeze Foams of above evaluations (CT/SEM), foaming and pore morphology evolution of another material specification (hydroxyapatite with reduced specific surface area/BET) and Freeze Foaming at different suspension temperatures. In addition, a correlation of Freeze Foams with varying distinctive structural features (porosity, pore size distribution etc.) and the effect on their mechanical stability will be made. Furthermore, other sizes and shapes of molds for foaming will be used and the filling procedure will be monitored and optimized in order to minimize/eliminate the inclusion of air into the suspensions.

## 5. Acknowledgements

The author very much appreciates the support and assistance of David Werner, the diploma student working within that DFG-funded project, and the project partner's *TUD-ILK* great assistance, work and many enlightening hours together as well as the DFG (Grant number 310892168) and Fraunhofer Society for funding this work.

## References

- [1] Schwartzwalder K, Somers A. Method of making porous ceramics articles. US Patent 3 090 094, 1963.
- [2] Komarneni S, Pach L, Pidugu R. Porous-alumina ceramics using bohemite and rice flour. *Mater. Res. Soc. Symp. Proc.*, Bd. 371, p. 285–290, 1995.
- [3] Lopes R A, Segadaes A M. Microstructure, permeability and mechanical behavior of ceramic foams. *Mater. Sci. Eng.*, Nr. 209, p. 149–155, 1996.
- [4] E. I. Du Pont de Nemours. Colloidal Silica Foam. UK Patent 1 175 760, 1967.
- [5] Wood L, Messina P, Frisch C. Method of preparing porous ceramic structures by firing a polyurethane foam that is impregnated with inorganic material. US Patent 3 833 386, 1974.
- [6] Eckert K-L, Mathey M., Mayer J, Homberger F, Thomann P., Groscurth P, Wintermantel E. Preparation and in vivo testing of porous alumina ceramics for cell carrier applications. *Biomater*, Nr. 21, pp. 63-69, 2000.
- [7] Moritz T. Lightweight green compact and molded article made of a ceramic and/or powder-metallurgical material, and the method for the production of thereof. DE102008000100, 2008.
- [8] Ahlhelm M. Gefrierschäume – Entwicklung von zellularen Strukturen für vielfältige Anwendungen/ Freeze Foams – Development of cellular structures for various applications. *Schriftenreihe Kompetenzen in Keramik*, Band 32, Hrsg.: Fraunhofer IKTS, Dresden; Alexander Michaelis, Fraunhofer Verlag, ISBN 978-3-8396-0977-4, 2016.
- [9] Ahlhelm M, Moritz T. Synthetic bone substitute material and method for producing the same. European Patent EP2682137A3, 2013.
- [10] Ahlhelm M, Moritz T. Herstellung eines biokompatiblen Hydroxylapatit-ZrO<sub>2</sub>-Hybridschaums über die Methode der Gefrier-Direktschäumung. *Schriftenreihe Werkstoffe und Werkstofftechnische Anwendungen* 41. Hrsg., B. Wielage, Hrsg. Chemnitz: Deutsche Gesellschaft für Materialkunde e.V. DGM, 2011.
- [11] Ahlhelm M, Gorjup E, von Briesen H, Moritz T, Michaelis, A. Freeze-foaming-a promising approach to manufacture strength enhanced ceramic cellular structures allowing the ingrowth and

differentiation of human mesenchymal stem cells. Faenza: Proceedings of MiMe-Materials in Medicine, International Conference 1st edition MIME, 2013.

[12] Ahlhelm M, Fruhstorfer J, Moritz T, Michaelis A. Die Herstellung von Feuerleichtsteinen über die Gefrier-Direktschäumungsmethode. *Keramische Zeitschrift* 2011, Bd. 6, Nr. 63:405-409.

[13] Ahlhelm M, Fruhstorfer J, Moritz T, Michaelis A. The Manufacturing of Lightweight Refractories by Direct Freeze Foaming Technique. *Interceram* 2011, Bd. 6, Nr. 60:394-399.

[14] Ahlhelm M, Günther P, Scheithauer U, Schwarzer E, Günther A, Slawik T, Moritz T, Michaelis A. Innovative and novel manufacturing methods of ceramics and metal-ceramic composites for biomedical applications. *J. Eur. Cer. Soc.* 2016, Bd. 36, Nr. 12:2883-2888.

[15] Ahlhelm M, Schwarzer E, Scheithauer U, Moritz T, Michaelis A. Novel ceramic composites for personalized 3D-structures, *Journal of Ceramic Science and Technology* 2017, Bd. 8, No.1:91-100.

[16] Routschka G. *Feuerfeste Werkstoffe*. Essen: 2. Auflage, Vulkan-Verlag, 1997.

[17] Best S M, et al. Bioceramics: Past, present and for the future. *J. Eur. Cer. Soc.*, 28, 1319–1327, 2008.

[18] Sepulveda P, et al. In vivo evaluation of hydroxyapatite foams. *J Biomed Mater Res.* 2002, Bd. 62, Nr.4:587-92.

[19] Rueger J M, Linhart W, Sommerfeldt D. Biologische Reaktionen auf Kalziumphosphatkeramik-Implantationen. Tierexperimentelle Ergebnisse. *Der Orthopäde* 1998, 27:89±95 © Springer-Verlag, 89-95.

[20] Nöbel D. Untersuchungen zur Osteointegration und Resorbierbarkeit von Implantatbeschichtungen für den Knochenersatz. Eine histologische und histomorphometrische Studie am Tiermodell. Dissertation, 2007.

[21] Schaller M. In situ Röntgen-CT Untersuchung des mechanischen Verhaltens eines Polymerhartschaumstoffes im Zugversuch. Hochschule Anhalt, 2009.

[22] Ohgaki T. In-situ High-resolution X-ray CT Observation of Compressive and Damage Behaviour of Aluminium Foams by Local Tomography Technique. *Advanced Engineering Materials* 2006, Bd. 8, Nr. 6:473–475.

[23] Ballaschk U B. Mg-PSZ Reinforced TRIP-Steel MMCs – In Situ CT Investigations of Cruciform Samples under Compressive Loading. *Adv. Eng. Mater.* 2013, Bd. 15, pp 590–599.

[24] Berek H B. In Situ Characterization of Internal Damage in TRIP-Steel/Mg-PSZ Composites under Compressive Stress Using X-Ray Computed Tomography. *Adv. Eng. Mater.* 2011, Bd. 13, pp 1101–1107.

[25] Mei H, Yu C, Xu Y, et al. Effect of impact energy on damage resistance and mechanical property of C/SiC composites under low velocity impact. *Materials Science and Engineering: A* 2017, Bd. 687, pp 141-147.

[26] Fraunhofer ITWM, Department of Image Processing (2005) MAVI – Modular Algorithms for Volume Images. <http://www.itwm.fraunhofer.de/bv/projects/MAVI/>

[27] <https://www.volumegraphics.com/de/produkte/vgstudio.html>

[28] Hufenbach W M: A test device for damage characterisation of composites based on in situ computed tomography. *Composites Science and Technology* 2012, Bd. 72, pp 1361–1367.

[29] Böhm R, et al. A quantitative comparison of the capabilities of in situ computed tomography and conventional computed tomography for damage analysis of composites. *Composites Science and Technology* 2015, Bd. 110, pp 62–68.